Published in final edited form as:
IEEE Trans Med Imaging. 2012 September ; 31(9): 1821–1832. doi:10.1109/TMI.2012.2205586.

Comb-push Ultrasound Shear Elastography (CUSE): A Novel Method for Two-dimensional Shear Elasticity Imaging of Soft Tissues

Pengfei Song [Student Member, IEEE], **Heng Zhao [Member, IEEE]**, **Armando Manduca [Member, IEEE]**, **Matthew W. Urban [Member, IEEE]**, **James F. Greenleaf [Life Fellow, IEEE]**, and **Shigao Chen [Member, IEEE]**
Department of Physiology and Biomedical Engineering, Mayo Clinic College of Medicine, Rochester, MN

Abstract

Fast and accurate tissue elasticity imaging is essential in studying dynamic tissue mechanical properties. Various ultrasound shear elasticity imaging techniques have been developed in the last two decades. However, to reconstruct a full field-of-view 2D shear elasticity map, multiple data acquisitions are typically required. In this paper, a novel shear elasticity imaging technique, comb-push ultrasound shear elastography (CUSE), is introduced in which only one rapid data acquisition (less than 35 ms) is needed to reconstruct a full field-of-view 2D shear wave speed map (40 mm × 38 mm). Multiple unfocused ultrasound beams arranged in a comb pattern (comb-push) are used to generate shear waves. A directional filter is then applied upon the shear wave field to extract the left-to-right (LR) and right-to-left (RL) propagating shear waves. Local shear wave speed is recovered using a time-of-flight method based on both LR and RL waves. Finally a 2D shear wave speed map is reconstructed by combining the LR and RL speed maps. Smooth and accurate shear wave speed maps are reconstructed using the proposed CUSE method in two calibrated homogeneous phantoms with different moduli. Inclusion phantom experiments demonstrate that CUSE is capable of providing good contrast (contrast-to-noise-ratio ≥25 dB) between the inclusion and background without artifacts and is insensitive to inclusion positions. Safety measurements demonstrate that all regulated parameters of the ultrasound output level used in CUSE sequence are well below the FDA limits for diagnostic ultrasound.

Index terms

comb-push; unfocused ultrasound beam; ultrasound elastography; acoustic radiation force; inclusion

INTRODUCTION

In dynamic ultrasound elastography, soft tissue mechanical properties are characterized by inducing shear waves into the tissue and solving for shear modulus based on ultrasonically tracked shear wave motions [1]. Assuming soft tissues are incompressible, isotropic, linear, and elastic (i.e. with negligible shear wave dispersion), shear modulus, μ, is related to shear wave propagation speed, c_s, by:

Corresponding Author: Shigao Chen, Address: 200 First Street, S.W., Rochester, MN 55905 U.S.A., Phone: 507-284-8252, Fax: 507-266-0361, chen.shigao@mayo.edu.

$$\mu=\rho c_s^2 \quad (1)$$

where ρ is density and can be assumed to be 1000 kg/cm^3 for all soft tissues [2]. Therefore by estimating the induced shear wave propagation speed, the elastic shear modulus of the tissue can be recovered. In the past two decades, a variety of dynamic ultrasound elasticity imaging methods has been developed based on inducing shear waves either externally by mechanical vibrations or internally by acoustic radiation force. The acoustic radiation force methods are widely used in ultrasound elastography and therefore will be the focus of the short review here. Fatemi and Greenleaf [3] introduced vibro-acoustography and used two ultrasound transducers with slightly different frequencies to induce a low frequency acoustic response from the tissue which can be recorded by a hydrophone. Sarvazyan *et al.* [4] developed the shear wave elasticity imaging (SWEI) method which used acoustic radiation force to generate shear waves into the tissue and study tissue mechanical properties. Nightingale *et al.* [5] used acoustic radiation force as a remote palpation technique and developed acoustic radiation force imaging (ARFI). The ARFI sequence was also used to generate shear waves in their later studies [6]. Bercoff and Fink's group invented supersonic shear imaging (SSI) in which a quasi-plane shear wave was generated from multiple focused push beams marching axially. An ultrafast plane wave imaging technique was used to track shear wave motion generated by the SSI sequence and a frame rate of several kilohertz can be achieved [7]. McAleavey *et al.* induced a spatially-modulated impulse acoustic radiation force (SMURF) to generate shear waves with known spatial frequency and estimated shear wave temporal frequency by tracking shear wave motions, from which shear wave speed can be estimated [8]. Chen *et al.* developed shearwave dispersion ultrasound vibrometry (SDUV) which induced shear waves at multiple frequencies with acoustic radiation force to characterize tissue elasticity and viscosity using shear wave dispersion analysis [9]. Hazard *et al.* recently implemented acoustic radiation force to produce a synthetic crawling wave and solve for shear wave speed from the interfering crawling wave patterns[10, 11].

Ideally, fast data acquisition and rapid reconstruction of shear elasticity is desired for monitoring tissue dynamic mechanical properties in real time and minimizing motion artifacts. The frame rate of full field-of-view (FOV) two-dimensional (2D) shear elasticity imaging should only be limited by shear wave propagation speed within the tissue if computational time expenses can be made negligible. However, for elasticity imaging methods that use acoustic radiation force as the shear wave source, shear wave speed cannot be recovered within the push beam region due to absence of shear wave in this region (shear waves propagate away from the push beam center in opposite directions). Therefore a multiple data acquisition with different push beam locations is typically required to reconstruct a full FOV 2D shear elasticity map [12].

Recently, a new method of shear wave generation using an unfocused ultrasound beam was developed by Zhao *et al.* [13]. It has been shown that consistent shear wave speed measurements can be obtained at different depths using unfocused push beams. Because only one sub-aperture of transducer elements (8 to 16 elements) is used for each push beam, multiple sub-apertures of elements at different spatial locations can be used to simultaneously transmit unfocused push beams, which is called "comb-push" [14]. Comb-push was firstly used as alternative push beamforming for SMURF and the shear wave speed calculation technique is the same as SMURF [14]. In this paper, the comb-push technique is developed into a novel 2D shear elasticity imaging method called comb-push ultrasound shear elastography (CUSE) – targeting two difficulties in current shear elasticity imaging techniques: 1. Absence of shear waves in push beam region, and 2. Significant shear wave attenuation in areas that are far away from the push beam region. In CUSE, shear waves produced by each push beam can be treated as an independent realization of a

single unfocused push. Shear waves from different unfocused push beams interfere with each other constructively and destructively and eventually fill the entire FOV. To achieve robust shear wave speed estimation, a directional filter was used to extract left-to-right (LR) propagating shear waves and right-to-left (RL) propagating shear waves from the interfering shear wave patterns. A time-of-flight based shear wave speed estimate method was used to recover local shear wave speed at each pixel from both LR waves and RL waves. A final shear wave speed map is then composed from the LR speed map and RL speed map. Since comb-push produces shear wave motions with sufficient amplitude (about 10 μm at a depth of 20 mm in a phantom with Young's modulus of 6.8 kPa) at all image pixels including the push beam areas, not only can shear wave speed in "source free" areas be recovered, but shear wave speed in the push beam area can be recovered as well. This enables a full FOV 2D reconstruction of shear elasticity map with only one data acquisition (less than 35 ms). Homogeneous phantom experiments showed that CUSE is capable of producing a smooth 2D full FOV shear wave speed map with accurate shear wave speed estimates compared with magnetic resonance elastography (MRE) and 1D transient elastography (1D TE). Inclusion phantom experiments showed that CUSE is able to provide good contrast (contrast-to-noise-ratio ≥25 dB) between the inclusion and background without artifacts and is insensitive to inclusion locations. Safety measurements demonstrate that all regulated parameters of the ultrasound output level used in the CUSE sequence are well below the FDA limits for diagnostic ultrasound.

In this paper, we first introduce the principles of CUSE, including the realization of the comb-push sequence, shear wave motion detection, directional filter implementation and post-processing for 2D shear wave speed map reconstruction. We then provide results from phantom experiments including both homogenous and inclusion phantoms. Finally safety measurements on the CUSE sequence are described.

MATERIALS AND METHODS

Principles of comb-push

A Verasonics ultrasound system (Verasonics Inc., Redmond, WA) was used in this study to produce comb-push beams and track shear wave motion with a linear array transducer L7-4 (Philips Healthcare, Andover, MA). In comb-push, the elements of the linear array transducer (center frequency = 5 MHz) were divided into nine subgroups and labeled from subgroup no. 1 to no. 9, as shown in Fig. 1(a). Subgroups 1, 3, 5, 7 and 9 (12 elements in each subgroup) simultaneously transmit unfocused push beams (center frequency = 4.09 MHz, 600 μs duration), while subgroups 2, 4, 6 and 8 (17 elements in each subgroup) were turned off. Each subgroup of the push beam looks like a tooth of a comb, thus we call this kind of push a "comb-push". In this case, since five teeth (subgroups) were used, it is called a "5-tooth comb-push".

After comb-push transmission, the Verasonics system immediately switched to plane wave imaging mode with all transducer elements (center frequency = 5 MHz), as shown in Fig. 1(b). A plane wave imaging compounding method was used to improve the signal-to-noise-ratio (SNR) of shear wave displacement tracking [15]. In this study, we compounded three frames at three different steering angles (−4°, 0°, 4°) to obtain one imaging frame, with an effective frame rate of 3745.32 Hz and spatial pixel resolution of one ultrasound wavelength (~0.308 mm assuming ultrasound speed c = 1540 m/s). The FOV is 40 mm axially and 39 mm laterally. A total number of 121 frames were collected in each CUSE imaging sequence (less than 35 ms).

Field II simulation of comb-push radiation force field

The Field II simulation tool [16] was used in this study to simulate the acoustic radiation force field produced by comb-push. A 128 element linear array transducer (L7-4) with element size of 7 mm × 0.283 mm (height × width) and kerf width of 0.025 mm was simulated. Each element was numerically divided into 5 × 5 sub-elements. The elevational focus was fixed at 25 mm depth. The center frequency was 4.09 MHz. Two frequency dependent attenuations (α) were simulated: 0.5 dB/cm/MHz and 0.7 dB/cm/MHz. The same 5-tooth comb-push as shown in Fig. 1(a) was simulated: each tooth has 12 elements and transmits unfocused push beams simultaneously, while the elements in between teeth are turned off. The pressure field is calculated in a 45 mm × 20 mm × 40 mm (lateral (x) × elevational (y) × axial (z), axial direction starts from 2 mm) space with a spatial resolution of 0.2 mm. The sampling frequency was 100 MHz. The excitation signal was a sinusoidal wave with 20 μs duration. The intensity $\boldsymbol{I}$ (bold font indicates a vector) of the pressure field is derived by

$$\boldsymbol{I}=\frac{\boldsymbol{p}^2}{\rho c} \quad (2)$$

where $\boldsymbol{p}$ is the pressure. The acoustic radiation force density was calculated based on [17]

$$\boldsymbol{f}=\frac{2\alpha \boldsymbol{I}}{c} \quad (3)$$

The simulated acoustic intensity fields (normalized) in both x-z (mid-elevational) and y-z (in the center of subgroup 5) directions are shown in Fig. 2. Fig. 2(a) and (b) show the x-z and y-z plane of comb-push intensity field with 0.5 dB/cm/MHz attenuation; Fig. 2(c) and (d) show the intensity field with 0.7 dB/cm/MHz. The simulation results indicate that each single unfocused push beam can reach a depth of 30–40 mm. The spacing in between comb-push subgroups is sufficient to separate different unfocused push beams so that no beam-to-beam interference will occur. The y-z view shows a tightly -shaped beam profile throughout depth.

Acoustic field scan of comb-push

To compare with the simulation results, the acoustic output field of comb-push was scanned with a needle hydrophone. The needle hydrophone (HGL-0200, Onda Corporation, Sunnyvale, CA) was mounted on a mechanical stage which was controlled by stepper motors. The scan was performed in a water tank where the transducer repeatedly transmits comb-push beams (center frequency = 4.09 MHz) while the needle hydrophone was translated by the mechanical stage. Two-dimensional scans were performed for both x-z and y-z directions. The acoustic intensity map has the same dimension and resolution as the simulation map: x-z plane was 45 mm (x) by 40 mm (z) and y-z plane was 20 mm (y) by 40 mm (z), spatial resolution was 0.2 mm. The scanned acoustic intensity field (normalized) is shown in Fig. 3.

Particle velocity demodulation

Particle velocity (V_Z) caused by shear wave propagation was used for shear wave speed estimation. V_Z was calculated from in-phase/quadrature (IQ) data of consecutive frames using a one-dimensional autocorrelation method [18]. Three pixels in space and two sampling points in the slow time direction were used for averaging. A 3 × 3 pixel spatial median-filter (0.92 mm × 0.92 mm) was then used on each frame of the shear wave motion

image to remove noise spike points. The axial particle velocity of the proposed CUSE sequence in a homogenous phantom is shown in Fig. 4.

Directional Filtering

As shown in Fig. 4, each unfocused beam generates two shear wave fronts propagating towards opposite directions: left-to-right (LR) and right-to-left (RL). Shear waves from different teeth constructively and destructively interfere with each other (Fig. 4) and a complicated shear wave field is created. Although sufficient amount of shear waves have been produced into the medium, the destructive interference greatly decreases the amplitude of shear wave motion which will compromise the shear wave velocity estimate. To remove the destructive interference and separate LR and RL shear waves, a directional filter similar to [19, 20] was used in this study. The directional filtered particle axial velocity results at 9.24 mm depth are shown in Fig. 5. When performing a two-dimensional Fourier transform of the shear wave field as in Fig. 5(a), a symmetric spectrum can be obtained with the first and the third quadrant corresponding to the LR waves, the second and the fourth quadrant corresponding to the RL waves. A mask can be designed to zero-out the spectrum of the second and the forth quadrant to extract the LR waves (Fig. 5(b)); and a complementary mask will extract the RL waves (Fig. 5(c)). Comparing the shear wave field before and after directional filtering, one can see that all destructive shear wave interferences have been removed in both LR and RL shear wave fields.

Local Shear Wave Speed Recovery and 2D Shear Wave Speed Map Reconstruction

In this study, shear wave speed is estimated using the time-of-flight algorithm by cross-correlating recorded particle velocity profiles along the lateral direction. Two points separated by 8 ultrasound wavelengths (8 pixels) at the same depth are used to calculate local shear wave speed of the pixel in the middle [12]. The particle velocity profiles were Tukey windowed (the ratio of tapered section to constant section is 0.25 [21]) so that both ends of the signal were forced to be zero, facilitating more robust cross-correlation. The velocity profiles were interpolated by a factor of five before cross-correlation (i.e., using the ‘interp’ function in MATLAB).

An important advantage of CUSE imaging is that only one data acquisition is required to reconstruct a full FOV 2D shear wave speed map. Thanks to the directional filter, as shown in Fig. 6(a) and (b), one can observe that the LR waves propagate through subgroups no. 3, 5, 7, and 9 and RL waves propagate through subgroups no. 7, 5, 3, and 1. Because the push beam areas are covered by shear waves from other subgroups during wave propagation, shear wave speed at these areas can be recovered as well. One may notice that LR waves cannot cover tooth no. 1 region and RL waves cannot cover tooth no. 9 region due to absence of shear wave. The LR speed map and RL speed map are therefore combined so that a full FOV speed map can be obtained, as shown in Fig. 6(c). Subgroup 1 region is reconstructed using the RL wave and subgroup 9 is reconstructed using the LR wave. Images of the regions in the middle were reconstructed by averaging the shear wave speed estimates from both LR and RL waves.

Homogeneous phantom experiments

To test the accuracy of using CUSE to measure shear wave speed, two custom-made homogeneous elasticity phantoms (CIRS Inc., Norfolk, VA) with different shear moduli (the nominal Young’s modulus of phantom 1 is 5.8 kPa, phantom 2 is 9.7 kPa) were used in this study. Both phantoms have ultrasound attenuation of 0.4 dB/cm/MHz, density of 1030 kg/m^3 and sound speed of 1539.0 m/s. Shear wave speeds of both phantoms shear wave speeds were calibrated by MRE [22] and 1D transient elastography (1D TE) [23]. The details of MRE and 1D TE experiments have been described in Zhao *et al.* [24]. Shear wave speeds at

different frequencies were measured by MRE (150 Hz) and 1D TE (100 Hz). Shear wave dispersion analysis using two-dimensional Fourier transform [25] (Fig. 7) shows that both phantoms have little dispersion. Thus it is possible to compare shear wave speeds measured at different frequencies by MRE and 1D TE.

Safety measurements

To evaluate the safety of the proposed CUSE method, both ultrasound pressure generated by comb-push and temperature rise during the entire CUSE sequence were measured. For ultrasound pressure measurement, the same needle hydrophone was used as in the acoustic field scan. The output of the needle hydrophone was measured with a digital oscilloscope with a 50 Ω input impedance. Only one tooth of comb-push beams (subgroup 5) was measured in this study because all unfocused beams can be assumed to have the same acoustic pressure, as shown in both simulation and field scan. The ultrasound transmit voltage was ± 90 V which is the maximum voltage the system can provide. The needle hydrophone was centered both laterally and elevationally to the central tooth. The ultrasound pressure from 2 to 42 mm with 5 mm step size was measured. The mechanical index (*MI*), which provides an indicator for the likelihood of mechanical effects and the derated spatial peak time average intensity ($I_{SPTA,0.3}$), was calculated by

$$\mathrm{MI}=\frac{p_{r,0.3}}{\sqrt{f_0}} \quad (4)$$

where $p_{r,0.3}$ is the peak rarefactional pressure derated at a rate of 0.3 dB/cm/MHz in MPa and f_0 is the ultrasound frequency in MHz. The Food and Drug Administration (FDA) sets the limit for *MI* at 1.9 [26]. $I_{SPTA,0.3}$ is given by [26]

$$I_{SPTA,0.3}=I_{SPPA,0.3}\cdot PD\cdot PRF \quad (5)$$

where *PRF* is the pulse repetition frequency and the value is 1 Hz, $I_{SPPA,0.3} = \mathrm{PII}_{0.3}/\mathrm{PD}$. The parameter $I_{SPPA,0.3}$ is the derated spatial peak, pulse average intensity. The FDA sets the limit for $I_{SPPA,0.3}$ at 190 W/cm ^{2}, and $I_{SPTA,0.3}$ at 720 mW/cm ^{2}. PII is the pulse intensity integral [27]

$$PII=\frac{\int_{t_1}^{t_2} v_h^2(t)\,dt}{10^4\,\rho c M_L^2(f_c)} \quad (6)$$

where v_h is the measured hydrophone voltage, t_1 is the beginning of the toneburst, t_2 is the end of the toneburst, ρ is the medium mass density, c is the sound speed of the medium, and $M_L(f_c)$ is the hydrophone sensitivity at frequency f_c, and the 10^4 factor is added to convert from W/m^2 to W/cm^2. The pressures were derated by 0.3 dB/cm/MHz for the calculations of $\mathrm{MI}_{0.3}$, $I_{SPPA,0.3}$, and $I_{SPPA,0.3}$. The pressure waveforms were not linear and an example of the waveform with the highest intensity measured is depicted in Fig. 8. A few cycles have been shown to demonstrate the nonlinearity of the signal. Eqn (6) does not assume a linear waveform.

To measure temperature rise during the CUSE sequence, a 30 gauge type T thermocouple (Omega Engineering Inc., Stamford, CT) was sandwiched between the transducer and a piece of pork tenderloin (12 cm by 7 cm by 5 cm). The thermocouple was positioned in the center of the central beam (subgroup no. 5). A full CUSE sequence was executed. Five

repeated measurements were taken for each CUSE sequence. In addition, maximum temperature increase (ΔT) within tissue associated with a comb-push tooth was calculated using the following equation from Palmeri *et al.*[28]:

$$\Delta T = \frac{2\alpha I}{c_v} t \quad (7)$$

where α is the ultrasound attenuation, I is the I_{SPPA} intensity, t is the time of the ultrasound transmission, and c_V is the heat capacity per unit volume ($c_V = 4.2$ J/cm^3/°C). The equation neglects cooling due to heat conduction and blood perfusion, and therefore provides a worst case estimation. To be conservative, we used non-derated intensity and a α value of 0.7 dB/cm/MHz to calculate maximum heating in Eq. (7). The FDA regulates the temperature rise (TR) of tissue to be no more than 6 °C [29].

RESULTS

Homogeneous phantom experiments

Fig. 9 shows the 2D shear wave speed maps reconstructed from both phantoms using the proposed CUSE technique. No spatial smoothing filter was applied to these maps. To test the accuracy of shear wave speed measurements, a region-of-interest (ROI) from 5 mm to 35 mm in the lateral direction and from 10 mm to 35 mm in axial direction was selected on each shear wave speed map. The mean values of shear wave speed from this ROI are compared with the values from MRE (30 mm by 60 mm ROI, depth by width) and 1D TE (25 mm line ROI along axial direction and 5 measurements from different lateral locations), as shown in Fig. 10.

Inclusion phantom experiments

A CIRS inclusion phantom (Model 059, CIRS Inc., Norfolk, VA) was also tested in this study. This phantom is a breast elastography phantom (sound speed of 1540 m/s, ultrasound attenuation of 0.5 dB/cm/MHz, and density of 1030 kg/m^3) which has 13 spherical masses with different sizes and locations. The stiffness of the inclusions is about three times greater than the stiffness of the background. Using Eq. (1), the shear wave speed of the inclusion is thus about 1.73 times greater than that of the background. The same CUSE sequence as used in the homogeneous phantoms was performed in this experiment. To test if CUSE is sensitive to relative positions between the inclusion and the push beams, a mechanical stage was used to move the transducer horizontally so that the same inclusion is at different lateral locations with respect to the transducer, as shown in Fig. 11. For each position, the transducer was adjusted to be aligned with the central slice of the inclusion. Then a CUSE sequence was executed and a 2D shear wave speed map was reconstructed, as shown in Fig. 12.

As shown in Fig. 12, ROIs were selected to estimate shear wave speeds of the inclusion and background. The measured mean and standard deviation (std.) values of shear wave speed are summarized in Table I. Table I also shows the calcuated ratio of inclusion shear wave speed and background shear wave speed. Using data from Table I, we can calcuate that the average shear wave speed of the inclusion from 6 different positions is 3.37 m/s, background is 1.78 m/s, and the average ratio of inclusion and background is 1.90. In addition, a contrast-to-noise-ratio (CNR) between the inclusion and background for each imaging position was calculated, which is given by[30]:

$$CNR = \frac{|C_I - C_B|}{\sigma_B} \quad (8)$$

where C_I and C_B are the mean shear wave speed of the inclusion and background, respectively; σ_B is the standard deviation of the shear wave speed of the background. C_I, C_B and σ_B were measured using the same ROIs as in Fig. 12. The measured CNR values are converted to dB using $20\log_{10}(CNR)$ and are summarized in Table I. The CNRs are all greater than or equal to 25 dB, which suggests good contrast between the inclusion and background.

Safety measurements

The values of *MI*, I_{SPPA} and I_{SPTA} measured from 2 mm to 42 mm depth with 5 mm step size were plotted in Fig. 13. Different derating values of 0.3, 0.5, and 0.7 dB/cm/MHz have been used to demonstrate what the *in* situ intensities might be in tissues with varying levels of ultrasound attenuation. As shown in Fig. 13, *MI*, I_{SPPA} and I_{SPTA} decreased with depth and have the highest values about 7 mm from the transducer surface.

For *TR* measurements, five repeated trials were performed. The values of temperature rise for the five experiments are: 0.4 °C, 0.3 °C, 0.4 °C, 0.4 °C, and 0.4 °C. The mean temperature rise was 0.38 °C, with a standard deviation of 0.04 °C. The maximum temperature rise in tissue calculated by Eq. (7) is 0.17 °C.

Table II summarizes the measured safety parameters of CUSE sequence to compare with FDA regulatory limits.

DISCUSSION

This study shows promising results of using CUSE to reconstruct a full FOV 2D shear wave speed map from only one data acquisition. Current 2D shear elasticity imaging techniques typically require multiple data acquisitions of the shear wave field with different push beam locations to reconstruct a full FOV 2D map because of the absence of shear waves in the push beam area and attenuation far from the push beam area. CUSE is capable of filling the full FOV with shear waves without any “blind areas” by introducing multiple unfocused push beams at different spatial locations simultaneously. Robust estimates of shear wave speed, computed using the cross-correlation method, are enabled by a directional filter that enables CUSE to separate the LR waves and RL waves so that no shear wave interferences occur. Results of this study show that CUSE is able to accurately recover shear wave speed for all pixels within the FOV in less than 35 ms, providing a fast snapshot of the tissue mechanical property. Such quick measurements reduce motion artifact and provide methods of measuring dynamic changes in tissue properties such as during flexion of muscles.

Homogeneous phantom experiments demonstrate that CUSE is capable of providing accurate shear wave speed measurements within the FOV (Fig. 9) compared with MRE and 1D TE. Shear wave speeds at push beam areas were well recovered by CUSE, which demonstrates our assumption that shear waves from different push beam areas can propagate through each other’s sources and thus provide local estimates of shear wave speed there (Fig. 6). Shear wave speed measurements from CUSE are slightly higher than those from MRE and 1D TE (Fig. 10). For phantom 1, CUSE measurement is 1.97% higher than MRE and 4.73% higher than 1D TE. For phantom 2, CUSE measurement is 6.50% higher than MRE and 3.70% higher than 1D TE. One possible reason for this overestimate is the diffraction effect as introduced by Catheline *et al.* [31]. The diffraction effect similar to 1D TE may also exist in shear waves induced by CUSE. Each unfocused push beam of CUSE can be treated as an aperture with non-negligible size compared with shear wavelength. Shear waves induced by such apertures may have increased shear wave speed near the push beam area. Since five unfocused push beams were used in CUSE, higher shear wave speed may exist within a narrow neighborhood around each push beam. However, more than one

shear wave from multiple push beams are produced and shear waves from a distant push beam do not have a diffraction effect and so there are no obvious overestimate patterns surrounding the push beam area. Nevertheless, one may still expect a slight increase of shear wave speed estimate because of the diffraction effect. Further FEM studies and phantom experiments are needed to obtain more insights and provide possible corrections to the CUSE measurements.

In this study, a 5-tooth comb-push was used for all experiments. For a smaller number of push beams, less shear wave energy would be induced in the media and thus SNR would be lower. Moreover, all experiments in this study were performed on phantoms that are very elastic. Real tissues, however, are more viscous and with much higher shear wave attenuation. For a smaller number of push beams, the shear wave produced by each beam has to propagate further; thus more shear wave attenuation would occur. For more than five push beams, although more shear wave energy would be induced, the push beams may not be spatially separated well since the transducer is limited to 128 elements. As a consequence, shear waves from different push beams may not be well separated in time, which may compromise the shear wave speed estimate. The number of elements of each push beam was fixed to be 12 in this study. Less number of elements produces shear waves with lower amplitude which attenuate faster. More number of elements produces shear waves with wider wave-fronts which deteriorates the spatial resolution of the shear wave and thus compromises the ability to image local heterogeneities such as inclusions. A detailed discussion of using different numbers of elements in an unfocused push beam is given in[13].

The number of elements per push beam was set to 12 to produce shear waves of sufficient aptitude while allowing the placement of several push beams within the transducer aperture. The spacing between adjacent push beams should be adequate to allow clean separation of the ultrasound push beams. In addition, the spacing should be large enough to allow sufficient recovery of the region under a push beam before shear waves from adjacent push beams arrive. In this study, we used 12 elements for each push beam and 17 elements in between, so that the distance between adjacent push beams is 29 elements (~ 8.93 mm). For phantom 1 (shear wave speed is about 1.5 m/s), it took about 6.0 ms for shear waves to propagate from one push beam to the closest neighbor push beam, while the push beam region was fully recovered 1.8 ms after the push transmission. For phantom 2 (shear wave speed is about 1.9 m/s), it took about 4.7 ms for shear waves to propagate and 1.5 ms for push region to be fully recovered. Therefore spacing between adjacent push beams was adequate for these experiments. For stiffer phantoms/tissues with higher shear wave speed, larger spacing is generally preferred to avoid interference from push region recovery to time-of-flight analysis of shear wave speed through cross-correlation. However, push region recovery would also be faster for stiffer materials: the impact of push region recovery in the case of very stiff materials and narrow push beam spacing needs further investigations.

Inclusion phantom experiments show that CUSE is able to provide good contrast (CNR ≥25 dB) between inclusion and background. The results indicate that CUSE is not sensitive to relative positions between the inclusion and push beams: at all six different lateral positions, the inclusion can be well reconstructed and there is no artifact in the background. The inclusion was designed to be spherical and thus the image cross-section should be circular. The reconstructed inclusion is elliptical with shorter diameter along the lateral dimension. This could be caused by the 8-pixel window in lateral direction used in local shear wave speed recovery. Smaller windows give better spatial resolution however provide less robust shear wave speed estimates [32]. Thus the choice of an 8-pixel window is a tradeoff between spatial resolution and robust shear wave speed estimation. The inclusion appears noisier and more oblong in shape in imaging positions 5 and 6 in Fig. 12. One possible reason is that the

imaging plane did not align elevationally with the center of the inclusion at imaging position 5 and 6. The imaging plane was adjusted in the elevational direction to overlap with the center of the inclusion at position 1 and then moved to the following positions. Since the inclusion is spherical with a diameter of only 10 mm and the phantom surface is not level, it is possible that imaging planes 5 and 6 (with largest translations) were off-center to the inclusion along the elevational direction of the transducer. Consequently, the shape of the inclusion may not be well preserved and the inclusions appear to be noisier. The measured ratio of shear wave speed of the inclusion and background is 1.9, which is higher than the designed ratio of 1.73. This is caused by the overestimation of shear wave speed within the inclusion at several inclusion reconstructions, for example, position 3. The overestimation might be caused by the same diffraction effect as discussed above when the inclusion is positioned very close or directly under the push beam. Moreover, when the inclusion is positioned right under the unfocused push beam, different modes of shear waves with different velocities may be excited within the inclusion. Shear wave reflections within the inclusion and push-beam-induced compressional waves might also cause the overestimation of shear wave speed of the inclusion. Future study is needed to investigate these issues.

The echo SNR of the utilized Verasonics system is about 24 dB. The fact that shear modulus estimates show low variance in this study is partially because all experiments were conducted in phantoms that are elastic and have less attenuation to shear waves than real tissues. Meanwhile, since multiple push beams at different locations were used for CUSE, distance-dependent shear wave attenuation is less pronounced than methods with single-location push. Therefore the tissue/phantom within the FOV is illuminated with shear waves with relatively higher SNR by which more robust shear modulus estimates could be achieved.

The safety measurements in this study demonstrate that all regulated parameters of the ultrasound output level used in the CUSE sequence are well below the FDA limits for diagnostic ultrasound. From simulations and field scans, it can be seen that the five unfocused beams are well separated in space. Therefore it is reasonable to assume that it is sufficient to measure the ultrasound output of one push beam. The acoustic output measurements were performed in water according to the procedure recommended by FDA [27]. As shown in Fig. 8, the pressure waveforms were not linear. Excess attenuation of harmonics produced in water due to nonlinear propagation may lead to underestimation of expository parameters [33]. However, we expect that underestimation due to nonlinear effects in these output measurements will not be too large for *unfocused* beams used in this study, because the maximum pressure of these beams is relatively small and occurs at a short distance from the transducer surface (Fig. 8 and Fig. 13).

Since unfocused push beams were used in CUSE, depth penetration might be a limitation for CUSE. The frequency dependent attenuation of the homogeneous phantoms was 0.4 dB/cm/MHz and the inclusion phantom was 0.5 dB/cm/MHz, which are relatively low compared with attenuation that may occur in tissues (for example, around 0.7 dB/cm/MHz for breast and prostate). As indicated in Fig. 13, *in situ* intensity may decrease substantially when ultrasound attenuation increases. Therefore, penetration in tissues may be considerably less than 4 cm achieved in phantom imaging here. Further studies will be conducted to improve penetration of CUSE in tissues, such as lowering the push beam frequency and increasing the time duration of push beam transmission.

Only one data acquisition is required for CUSE, and the propagation speed of the shear wave becomes the fundamental limit of the frame rate of 2D shear elasticity imaging. In this study, data acquisition was 35 ms, which is sufficient for the shear wave from the leftmost push beam to propagate to the rightmost push beam at a speed of 1.5 m/s. Neglecting post-

processing time and probe heating, a maximum frame rate of 28 frames/second can be achieved for 2D shear elasticity imaging, which should be sufficient to monitor tissue mechanical properties in real time. The safety parameters under this mode, however, would have to be evaluated.

The shear wave speed estimates show particularly low variance in this study. One reason may be due to the use of comb push such that each pixel in the FOV has a shear wave source nearby to provide stronger signals for time-of-flight calculation. Another important factor is that these experiments were conducted in phantoms. These phantoms were relatively soft, with relatively low ultrasound attenuation (0.4–0.5 dB/cm/MHz) and shear wave attenuation. Unlike *in vivo* applications, there were no phase aberrations in these phantom experiments. Therefore, shear waves produced in this study were strong with a SNR of about 20 dB at the depth of 40 mm. Further studies should be conducted to evaluate degrade of performance in real tissues.

In future work, *in vitro* and *in vivo* tissue experiments using CUSE will be conducted. Due to the limited depth penetration of an unfocused ultrasound beam, it is challenging to implement CUSE in deep tissues such as liver, kidney, heart and spleen. However, since CUSE is capable of achieving a penetration of 4 cm with a linear array transducer (in phantoms with an attenuation coefficient of 0.4–0.5 dB/cm/MHz), it should be sufficient for shallow tissues such as skeletal muscle, thyroid, and breast. It has been shown in Zhao *et al.* [13] that robust shear wave speed measurement can be achieved in bicep muscle using a single unfocused push beam. Thus CUSE should be able to work in muscle tissues and provide 2D shear elasticity maps. Further studies will be required to appraise the usefulness of CUSE in other tissues such as thyroid, prostate, and breast.

CONCLUSIONS

This paper introduces a novel 2D shear elasticity imaging technique termed CUSE and demonstrates the feasibility of using CUSE to reconstruct a 2D shear wave speed map with only one data acquisition (less than 35 ms). This is, to our knowledge, the first time that a 2D full FOV shear wave speed map has been reconstructed from only one data acquisition of an acoustic radiation force induced shear wave field. Homogeneous and inclusion phantoms show that CUSE is able to accurately reconstruct 2D shear wave speed maps and provide good contrast between the inclusion and background without artifacts. Future work includes *in vitro* and *in vivo* experiments on tissues such as muscle and breast.

Acknowledgments

The authors thank Dr. R. Ehman and Dr. M. Yin for their help in MRE phantom experiments and R. Kinnick for his experimental assistance. This work was supported by the National Institutes of Health (NIH) under Grant EB02167 and Grant DK082408. The content is solely the responsibility of the authors and does not necessarily represent the official views of NIH. Mayo and some of the authors have financial interest in the technology described here.

References

1. Greenleaf JF, Fatemi M, Insana M. Selected methods for imaging elastic properties of biological tissues. Annual review of biomedical engineering. 2003; 5:57–78.
2. Yamakoshi Y, Sato J, Sato T. Ultrasonic imaging of internal vibration of soft tissue under forced vibration. IEEE transactions on ultrasonics, ferroelectrics, and frequency control. 1990; 37:45–53.
3. Fatemi M, Greenleaf JF. Ultrasound-stimulated vibro-acoustic spectrography. Science. Apr 3.1998 280:82–5. [PubMed: 9525861]

4. Sarvazyan AP, Rudenko OV, Swanson SD, Fowlkes JB, Emelianov SY. Shear wave elasticity imaging: a new ultrasonic technology of medical diagnostics. Ultrasound in medicine & biology. Nov.1998 24:1419–35. [PubMed: 10385964]
5. Nightingale KR, Palmeri ML, Nightingale RW, Trahey GE. On the feasibility of remote palpation using acoustic radiation force. The Journal of the Acoustical Society of America. Jul.2001 110:625–34. [PubMed: 11508987]
6. Nightingale K, McAleavey S, Trahey G. Shear-wave generation using acoustic radiation force: in vivo and ex vivo results. Ultrasound in medicine & biology. Dec.2003 29:1715–23. [PubMed: 14698339]
7. Bercoff J, Tanter M, Fink M. Supersonic shear imaging: a new technique for soft tissue elasticity mapping. IEEE transactions on ultrasonics, ferroelectrics, and frequency control. Apr.2004 51:396–409.
8. McAleavey SA, Menon M, Orszulak J. Shear-modulus estimation by application of spatially-modulated impulsive acoustic radiation force. Ultrasonic imaging. Apr.2007 29:87–104. [PubMed: 17679324]
9. Chen S, Urban MW, Pislaru C, Kinnick R, Zheng Y, Yao A, Greenleaf JF. Shearwave dispersion ultrasound vibrometry (SDUV) for measuring tissue elasticity and viscosity. IEEE transactions on ultrasonics, ferroelectrics, and frequency control. Jan.2009 56:55–62.
10. Hah Z, Hazard C, Mills B, Barry C, Rubens D, Parker K. Integration of crawling waves in an ultrasound imaging system. Part 2: signal processing and applications. Ultrasound in medicine & biology. Feb.2012 38:312–23. [PubMed: 22178168]
11. Hazard C, Hah Z, Rubens D, Parker K. Integration of crawling waves in an ultrasound imaging system. Part 1: system and design considerations. Ultrasound in medicine & biology. Feb.2012 38:296–311. [PubMed: 22178166]
12. Tanter M, Bercoff J, Athanasiou A, Deffieux T, Gennisson JL, Montaldo G, Muller M, Tardivon A, Fink M. Quantitative assessment of breast lesion viscoelasticity: initial clinical results using supersonic shear imaging. Ultrasound in medicine & biology. Sep.2008 34:1373–86. [PubMed: 18395961]
13. Zhao, H.; Song, P.; Urban, MW.; Greenleaf, JF.; Chen, S. Shear Wave Speed Measurement Using an Unfocused Ultrasound Beam. Ultrasound in medicine & biology. online available: http://dx.doi.org/10.1016/j.ultrasmedbio.2012.05.015
14. Zhao H, Song P, Urban MW, Greenleaf JF, Chen S. Robust Shear Wave Speed Measurement Using Comb-push Ultrasound Radiation Force. IEEE transactions on ultrasonics, ferroelectrics, and frequency control. under review.
15. Tanter M, Bercoff J, Sandrin L, Fink M. Ultrafast compound imaging for 2-D motion vector estimation: application to transient elastography. IEEE transactions on ultrasonics, ferroelectrics, and frequency control. Oct.2002 49:1363–74.
16. Jensen JA, Svendsen NB. Calculation of pressure fields from arbitrarily shaped, apodized, and excited ultrasound transducers. IEEE transactions on ultrasonics, ferroelectrics, and frequency control. 1992; 39:262–7.
17. Palmeri ML, Sharma AC, Bouchard RR, Nightingale RW, Nightingale KR. A finite-element method model of soft tissue response to impulsive acoustic radiation force. IEEE transactions on ultrasonics, ferroelectrics, and frequency control. Oct.2005 52:1699–712.
18. Kasai C, Namekawa K, Koyano A, Omoto R. Real-time two-dimensional blood flow imaging using an autocorrelation technique. IEEE Transactions on sonics and ultrasonics. May.1985 SU-32:7.
19. Deffieux T, Gennisson JL, Bercoff J, Tanter M. On the effects of reflected waves in transient shear wave elastography. IEEE transactions on ultrasonics, ferroelectrics, and frequency control. Oct. 2011 58:2032–5.
20. Manduca A, Lake DS, Kruse SA, Ehman RL. Spatio-temporal directional filtering for improved inversion of MR elastography images. Medical image analysis. Dec.2003 7:465–73. [PubMed: 14561551]
21. Harris FJ. Use of Windows for Harmonic-Analysis with Discrete Fourier-Transform. Proceedings of the Ieee. 1978; 66:51–83.

22. Muthupillai R, Lomas DJ, Rossman PJ, Greenleaf JF, Manduca A, Ehman RL. Magnetic resonance elastography by direct visualization of propagating acoustic strain waves. Science. Sep 29.1995 269:1854–7. [PubMed: 7569924]

23. Sandrin L, Tanter M, Gennisson JL, Catheline S, Fink M. Shear elasticity probe for soft tissues with 1-D transient elastography. IEEE transactions on ultrasonics, ferroelectrics, and frequency control. Apr.2002 49:436–46.

24. Zhao H, Song P, Urban MW, Kinnick RR, Yin M, Greenleaf JF, Chen S. Bias observed in time-of-flight shear wave speed measurements using radiation force of a focused ultrasound beam. Ultrasound in medicine & biology. Nov.2011 37:1884–92. [PubMed: 21924817]

25. Bernal M, Nenadic I, Urban MW, Greenleaf JF. Material property estimation for tubes and arteries using ultrasound radiation force and analysis of propagating modes. The Journal of the Acoustical Society of America. Mar.2011 129:1344–54. [PubMed: 21428498]

26. Herman BA, Harris GR. Models and regulatory considerations for transient temperature rise during diagnostic ultrasound pulses. Ultrasound in medicine & biology. Sep.2002 28:1217–24. [PubMed: 12401393]

27. AIUM/NEMA. Standard for real-time display of thermal and mechanical acoustic output indices on diagnostic ultrasound equipment. Revision 2. AIUM; Laurel, MD: 2009.

28. Palmeri ML, Nightingale KR. On the thermal effects associated with radiation force imaging of soft tissue. IEEE transactions on ultrasonics, ferroelectrics, and frequency control. May.2004 51:551–65.

29. FDA. Information for manufacturers seeking marketing clearance of diagnostic ultrasound systems and transducers. Food and Drug Administration, Center for Devices and Radiological Health; Silver Spring, MD: 2008.

30. Hendrick, RE.; Raff, U.; Stark, DD.; Bradley, WG. Magnetic Resonance Imaging. 2. St. Louis: Mosby; 1992.

31. Catheline S, Wu F, Fink M. A solution to diffraction biases in sonoelasticity: the acoustic impulse technique. The Journal of the Acoustical Society of America. May.1999 105:2941–50. [PubMed: 10335643]

32. McLaughlin J, Renzi D. Using level set based inversion of arrival times to recover shear wave speed in transient elastography and supersonic imaging. Inverse Problems. Apr.2006 22:707–725.

33. Duck FA. Estimating in situ exposure in the presence of acoustic nonlinearity. Journal of ultrasound in medicine : official journal of the American Institute of Ultrasound in Medicine. Jan. 1999 18:43–53. [PubMed: 9952079]

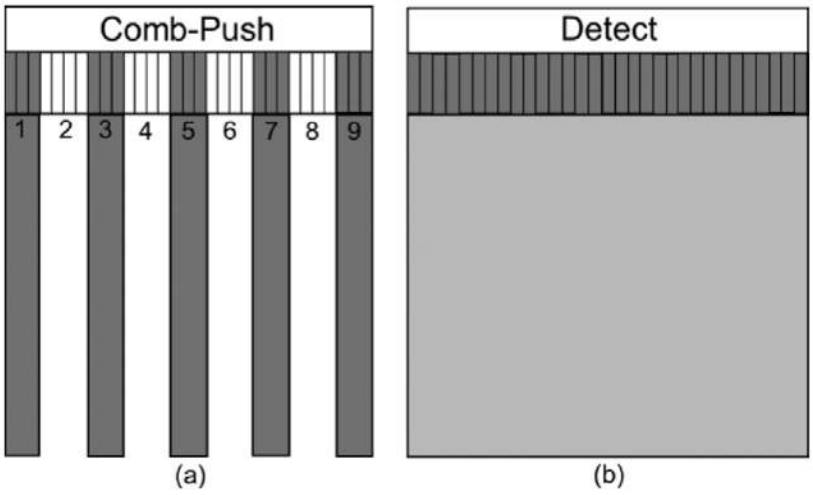

Figure 1.

Schematic plot of CUSE imaging sequence. (a) Comb-push is formed by transmitting unfocused push beams from subgroups 1, 3, 5, 7, and 9 (12 elements in each subgroup) simultaneously, while subgroups 2, 4, 6, and 8 (17 elements in each subgroup) are turned off. (b) All transducer elements are used in plane wave imaging mode for shear wave motion detection

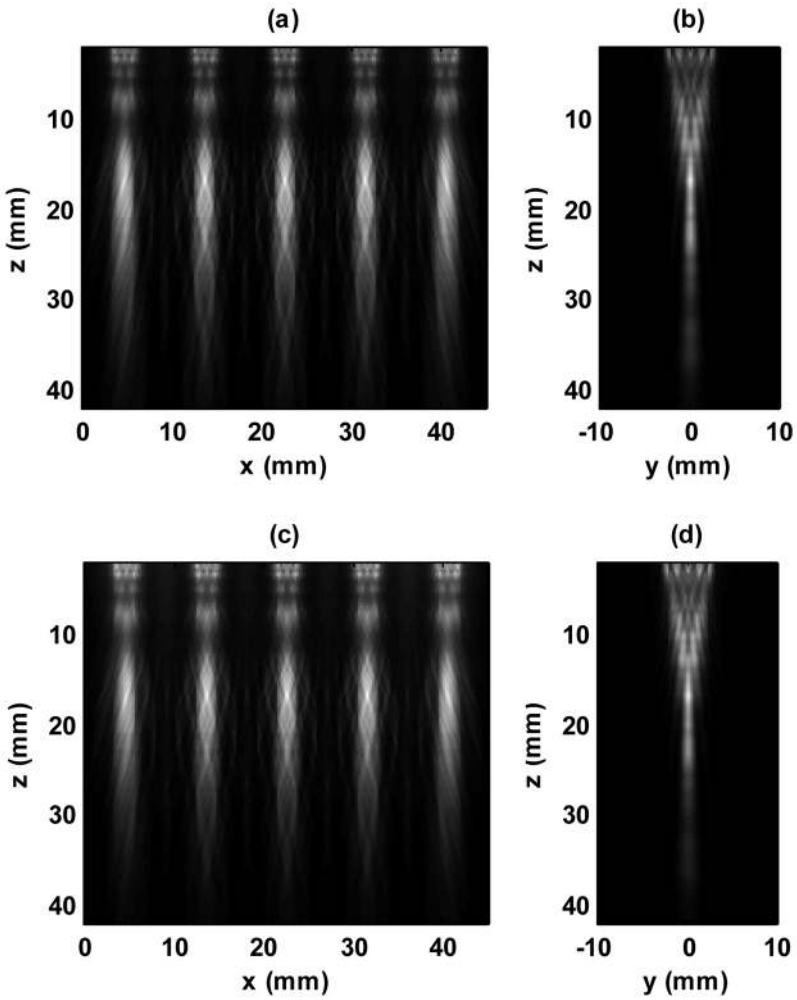

Figure 2.
Field II simulation of the acoustic radiation force field produced by comb-push. (a) Normalized intensity in x-z view for attenuation of 0.5 dB/cm/MHz. (b) Normalized intensity in y-z view for attenuation of 0.5 dB/cm/MHz. (c) Normalized intensity in x-z view for attenuation of 0.7 dB/cm/MHz. (d) Normalized intensity in y-z view for attenuation of 0.7 dB/cm/MHz.

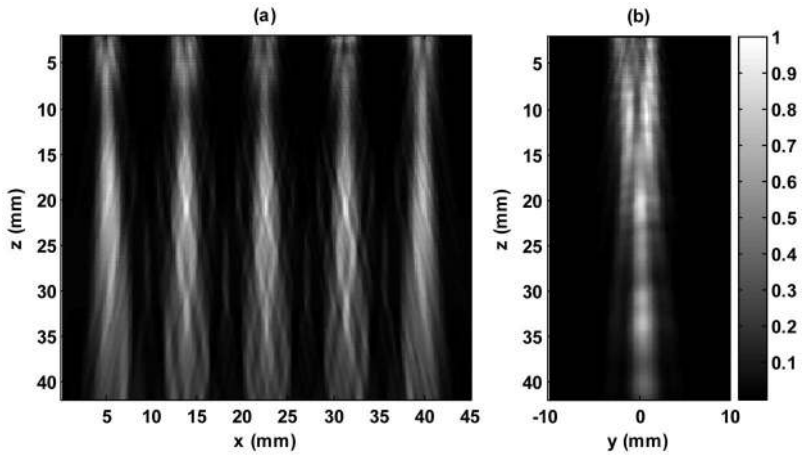

Figure 3.
Normalized acoustic intensity field of the comb-push beams. (a) x-z plane, (b) y-z plane. The color scale is the same for both figures.

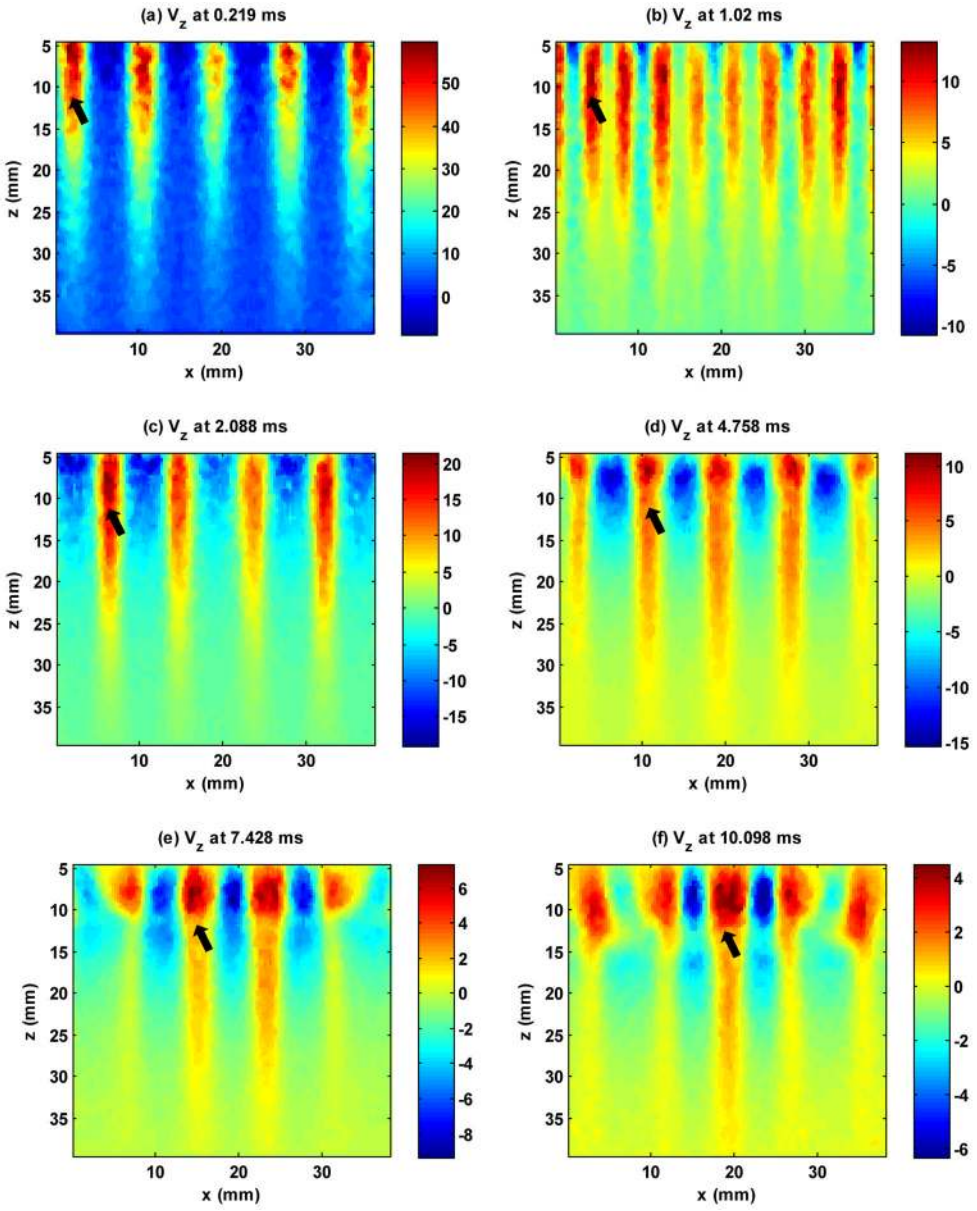

Figure 4.

Plots of particle axial velocity at different time steps. The shear waves constructively and destructively interfere with each other until all shear waves have passed through the FOV (only part of the shear wave propagation plots are shown here for succinctness). The black arrows indicate the left-to-right propagating shear wave front from the leftmost tooth (subgroup 1) of the comb-push. The color-bar is in unit of mm/s and is different for each time point. (a) initial positions of shear waves produced by 5 teeth, black arrow is at the shear wave front from subgroup 1 of the comb-push, (b) shear waves from each push beam begin to propagate away from the push beam on opposite directions, the right-propagating shear wave from subgroup 1 was pointed by the black arrow, (c) the right-propagating shear wave from subgroup 1 merged with the left-propagating shear wave from subgroup 3, (d) the right-propagating shear wave from subgroup 1 merged with the left-propagating shear wave from subgroup 5, (e) the right-propagating shear wave from subgroup 1 merged with

the left-propagating shear wave from subgroup 7, (f) the right-propagating shear wave from subgroup 1 merged with the left-propagating shear wave from subgroup 9.

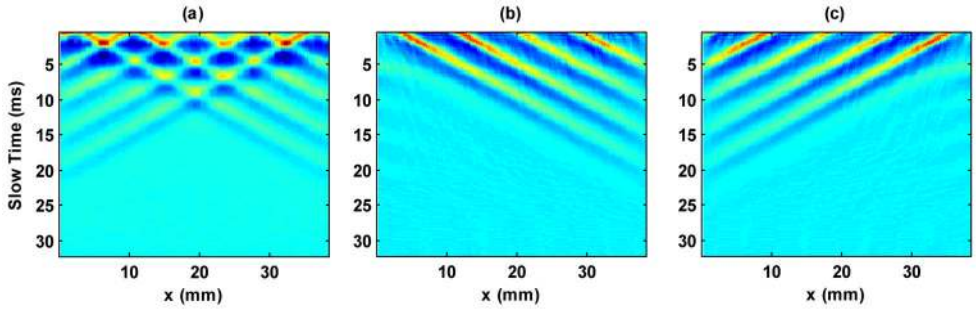

Figure 5.
Particle axial velocity plots along slow-time and lateral dimensions before and after directional filtering. (a) Before directional filtering, the complex shear wave field with constructive and destructive shear wave interference can be observed. (b) LR shear waves extracted by directional filter. All shear waves are propagating from left to right and no destructive interference with RL waves can be observed. (c) RL shear waves extracted by directional filter. Again all destrutive shear wave interferences have been removed.

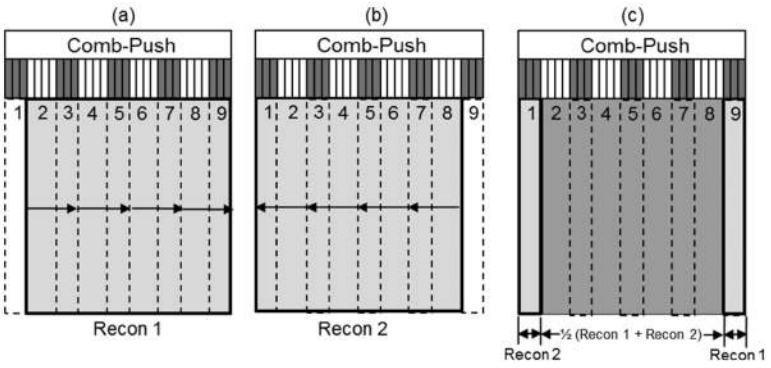

Figure 6.

Schematic plots of 2D shear wave speed map reconstruction. (a) Shear wave speed map reconstructed using LR waves, (b) shear wave speed map reconstructed using RL waves, (c) final shear wave speed map combined by Recon1 and Recon2. Subgroup 1 area is recovered from Recon2, subgroup 9 area is recovered from Recon1, while the area in the middle is recovered from averaging Recon1 and Recon2.

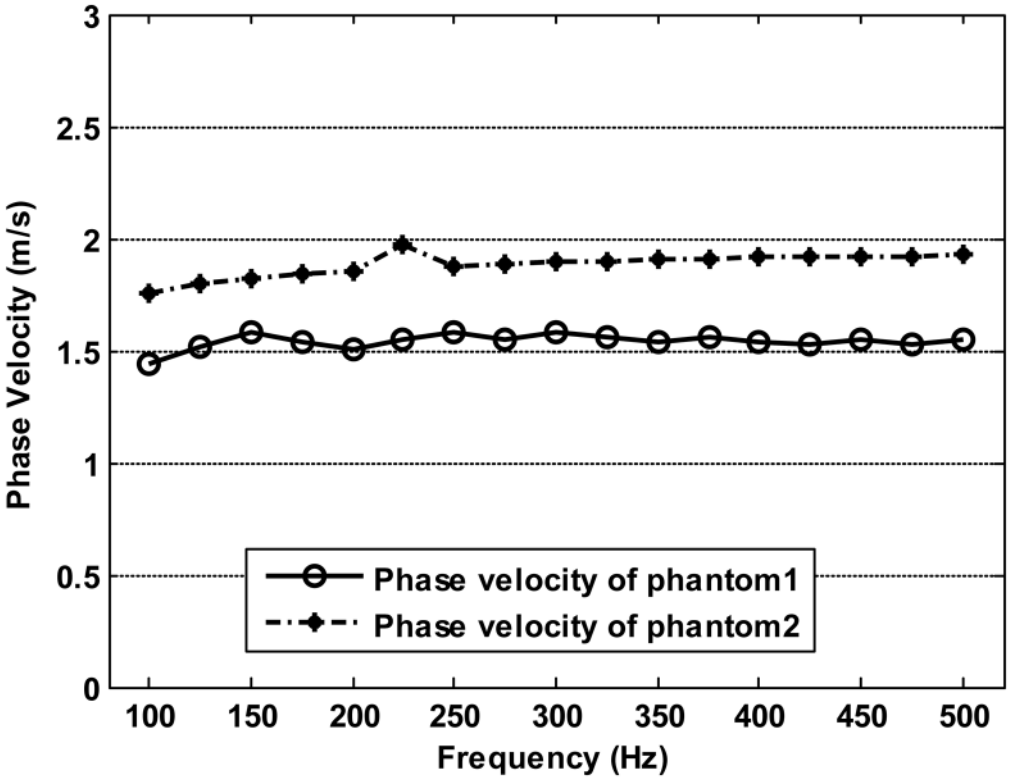

Figure 7.
Shear wave dispersion analysis for phantom 1 and phantom 2. Shear wave speeds at different frequencies were measured using two-dimensional Fourier analysis.

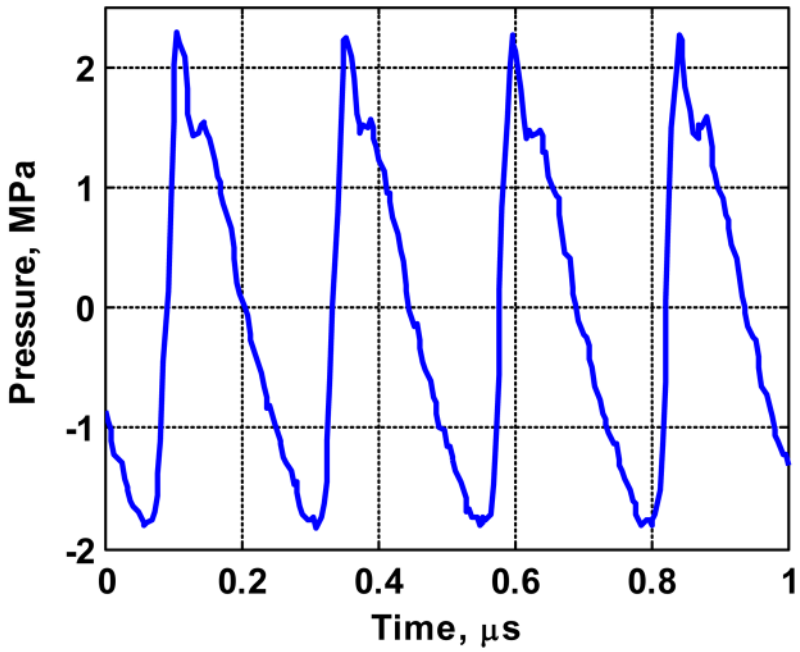

Figure 8.
Maximum measured pressure waveform for the unfocused beam (derated with 0.3 dB/cm/MHz to the depth of 7 mm where the maximum pressure located in water).

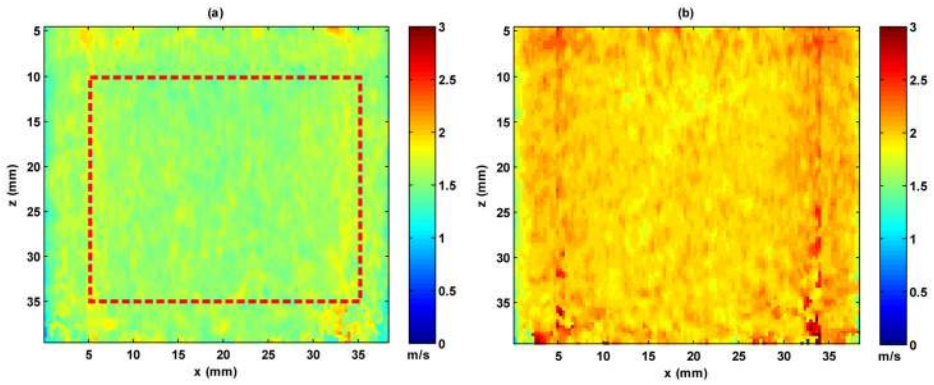

Figure 9.

2D shear wave speed maps from two CIRS phantoms with different moduli. (a), shear wave speed map of phantom 1, the red rectangle indicates the measuring ROI, (b) shear wave speed map of phantom 2, the measuring ROI is the same as in (a).

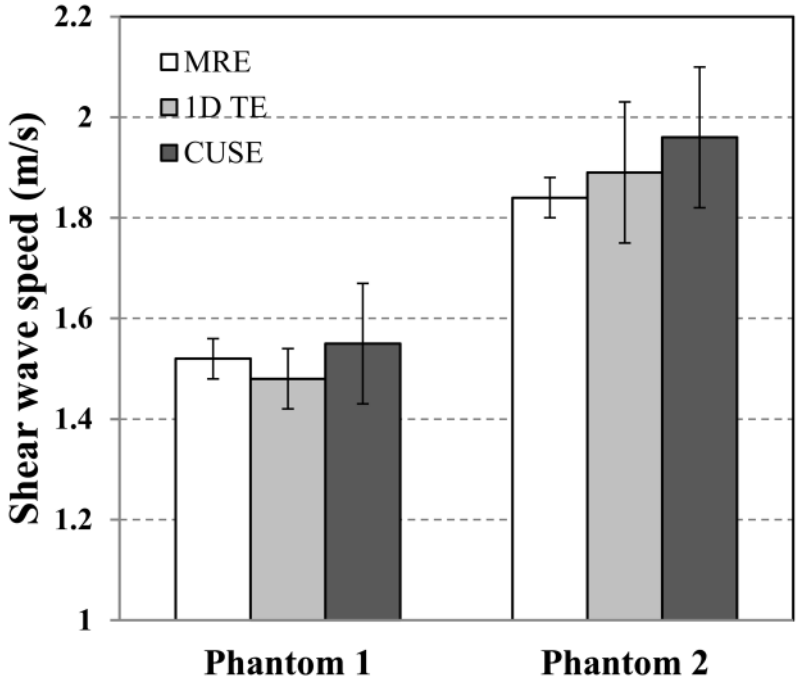

Figure 10.
Shear wave speed of phantom1 and phantom2 measured by MRE, 1D TE and CUSE. Error bars are plotted from 95% confidence interval (CI).

Figure 11.
A CIRS breast elastography phantom was imaged using CUSE. The ultrasound transducer was mounted on a mechanical stage. By translating the transducer, the inspected inclusion will change its relative position to the transducer.

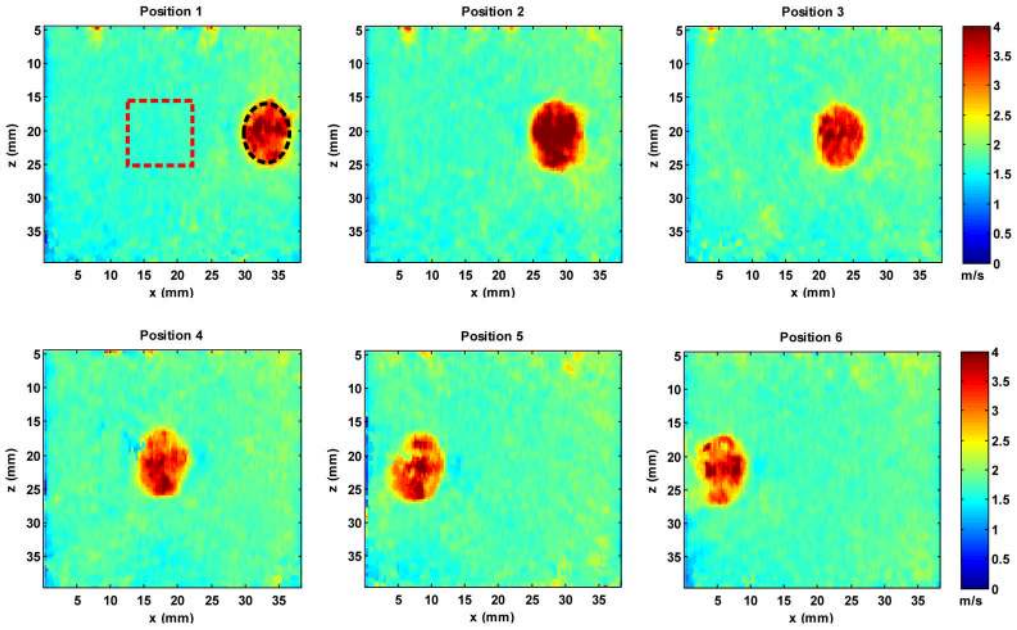

Figure 12.

Reconstructed 2D shear wave speed maps for the CIRS breast elastography phantom at different lateral positions (from Position 1 to Position 6). All shear wave speed maps are under the same color scale. For each position, a black circular ROI within the inclusion and a red rectangular ROI in the background were drawn to estimate shear wave speed, as shown in the plot of Position 1. Similar ROIs were selected for the rest positions.

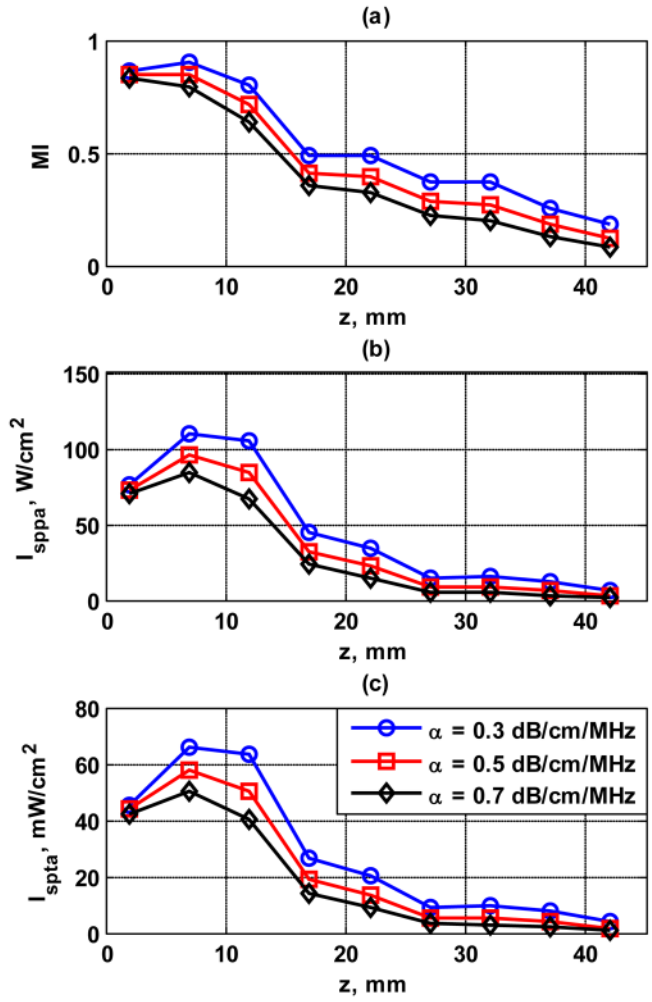

Figure 13.
Acoustic output results for different levels of deration (0.3, 0.5, 0.7 dB/cm/MHz). (a) *MI*, (b) I_{SPPA}, (c) I_{SPTA}.

Table I

Shear wave speed and CNR on measurements of the inclusion and background from different positions.

	Inclusion (m/s) mean ± std.	Background (m/s) mean ± std.	Inclusion/Background	CNR (dB)
Position 1	3.32 ± 0.48	1.72 ± 0.09	1.93	25
Position 2	3.95 ± 0.49	1.73 ± 0.07	2.28	30
Position 3	3.41 ± 0.34	1.75 ± 0.07	1.95	28
Position 4	3.26 ± 0.40	1.88 ± 0.08	1.73	25
Position 5	3.19 ± 0.46	1.82 ± 0.07	1.75	26
Position 6	3.11 ± 0.46	1.79 ± 0.06	1.74	27

Table II

Summary of measured safety parameters of CUSE sequence compared with FDA regulatory limit

Safety Parameter	Maximum Values Measured	FDA Regulatory Limit
$MI_{0.3}$	0.9	1.90
$I_{SPPA,0.3}$ (W/cm^2)	109.4	190
$I_{SPTA,0.3}$ (mW/cm^2)	65.63	720
TR (°C)	0.4	6